ZANCO Journal of Pure and Applied Sciences
The official scientific journal of Salahaddin University-Erbil
https://zancojournals.su.edu.krd/index.php/JPAS

ISSN (print):2218-0230**, ISSN (online):** 2412-3986**, DOI: http://dx.doi.org/10.21271/zjpas**

RESEARCH PAPER

The influence of non-sinusoidal voltage sources on the steady state performance of different NEMA Designs of IMs

Nihaya Abdulghafoor Othman[1], Hilmi Fadhil Ameen[2]

Department of Electrical Engineering, College of Engineering, Salahaddin University-Erbil, Kurdistan Region, Iraq

A B S T R A C T:

Voltage distortion has become one of the most common power quality problems in industrial applications, which has gained a great deal of attention in recent years because of the widespread usage of non-linear loads. Three-phase induction motors are widely used and one of the factors that confirm the reduction of their performance is the presence of harmonics in their voltage supply. In this paper, the impact of non-sinusoidal supply voltages on the steady-state performance of different NEMA designs of squirrel cage induction motors (SCIMs) is presented. It presents the analytical modeling based on the equivalent circuit taking into consideration the skin effect impedance that incorporates the skin effect on the rotor bars, which is used to investigate the motor performance under such conditions. The importance of this study is that it compares all NEMA designs in terms of electromagnetic torque, efficiency, losses, power factor, stator and rotor currents, and derating factor under a distorted supply voltage that is polluted by the most significant odd harmonic orders at adjustable levels in the range of (0–25) % of THD_v%. The obtained results are compared and validated with the system employed by using MATLAB/Simulink software. The simulation and the analytical model results have shown good accuracy.

KEY WORDS: *Induction motor, NEMA design, non-sinusoidal supply, THD, skin effect.*
DOI: http://dx.doi.org/10.21271/ZJPAS.34.6.2
ZJPAS (2022) , 34(6);8-19 .

1. INTRODUCTION:

The most important loads used in the electric power system are electric motors, which in industrial applications consume about 40% of all the generated electrical energy worldwide (Ruthes et al., 2016). Among them, squirrel cage induction motors (SCIMs) are extensively used in a variety of industrial applications such as centrifugal pumps, industrial drives, large blowers and fans, machine tools, lathes, , and other turning equipment due to their characteristics such as simple and robust structure, low cost, wide speed adjustment, minimal maintenance need, wide power range, reliable operation, and mass production technology (Tezcan et al., 2018).

Besides their advantages, SCIMs have a drawback, which is poor starting torque. There is a limit to the use of SCIMs in some areas that require high starting torque. Therefore, to improve the starting and normal operating characteristics, SCIMs can be classified into different designs according to rotor construction by adjusting the resistance and reactance of the rotor through the design of the rotor bars of SCIMs. NEMA standards mainly specify four design types for induction motors: Design A, B, C, and D. These categories are characterized by the rotor slot shape and torque-speed characteristics. Design A has low rotor resistance and low leakage inductance with simple deep bar designs, and their running efficiency is good, but they require a considerable current to start. Design B has a deep bar cage and minimal operating slip. The motors of design D have a very high starting torque, high operating slip, and low efficiency. Design C differs from the

*** Corresponding Author:**
Nihaya Abdulghafoor Othman
E-mail: nihaya.othman@su.edu.krd
Article History:
Received: 23/05/2022
Accepted: 28/07/2022
Published: 20/12 /2022

others in that it has a double cage rotor slot, a strong starting torque, and a low operating slip (Neapolitan and Nam, 2018).

In the last few decades, the electrical power system has grown in complexity at a rapid rate. Modern power electronic converters create a wide range of harmonic components and distort both in current and voltage, which degrades the quality of provided energy, increase energy losses, and further decrease power system reliability. Distorted voltages have a negative impact on other loads, particularly electrical motors, which are fed from the point of common coupling (PCC) (Deraz and Azazi, 2017). Due to the rise in iron and copper losses at the harmonic frequencies, the operation of motors on a polluted harmonic system reduces the machine's efficiency and service life. Additionally, voltage and current harmonics might influence the produced torque. Moreover, in rotating machinery, harmonics may create vibrations and noise. Negative sequence harmonics give the motor a negative torque that goes against the fundamental torque. This makes the motor less efficient (Beleiu et al., 2020).

The harmonic effects on SCIMs are very relevant due to the growing use of non-linear loads in grids. Many researchers have looked into it, with several studies focusing on the operation of IMs under non-sinusoidal supply voltages. (Pedra et al., 2006) have proposed an IM model for the study of harmonic load flow in balanced and unbalanced conditions. (Debruyne et al., 2012) have compared the effects of harmonic voltage distortion and harmonic content phase angle on the overall motor efficiency of line-start permanent magnet machines (LSPMM) and IM. **The impacts of voltage unbalance and distorted supply on the performance of IMs have been studied by** (Donolo et al., 2016), (Neves et al., 2016) and (Deleanu et al., 2019). (Lerch and Rad, 2016) have studied the power losses in IMs supplied with distorted voltage, same study has been done by (Zhang et al., 2017) and (Donolo et al., 2020) when IM is supplied with unbalanced and distorted voltage. (Beleiu et al., 2020) have investigated the effects of harmonics not only on the technical features of the IM but also on the power supply and the mechanical drive system. (Gnaciński and Klimczak, 2020) have investigated the influence of subharmonics on speed fluctuations, currents, power losses, and torque pulsations of IM. (Lordoglu et al., 2021) have analyzed different cage rotor IMs in terms of electromagnetic and mechanical operational performance, space harmonic and adverse magnetic noise influences in order to improve performance in an electric vehicle. (Ameen and Aula, 2021) and (Hilmi and Fadhil, 2021) have investigated the steady state performance of a slip power recovery and static rotor resistance control of IM drive system under unbalanced supply voltage and evaluated the impact of voltage unbalance and firing angle of the inverter and duty cycle on the chopper circuit on the THD of stator and rotor currents. (Jassim et al., 2021) have investigated the performance of a three-phase IM under the influence of balanced and unbalanced distorted voltages.

This paper has investigated the influence of distorted supply on the steady-state performance of all NEMA designs of SCIMs corresponding to the skin effect. The system is modeled using the analytical method to predict the effect of harmonics and are validated by using MATLAB/Simulink. The three-phase supply, which is distorted by odd harmonics, is fed to the IM to study electromagnetic developed torque, stator and rotor current, losses, efficiency, power factor, and derating factor.

2. The methodology

For induction motors, two types of harmonics are investigated: space harmonics and time harmonics. When the power supply is sinusoidal, space harmonics are produced owing to the interaction of the various phase windings. This form of harmonic will affect the starting of a motor and generate magnetic noise and vibration. Time harmonics are generated directly by the power supply when non-sinusoidal currents are supplied to IMs (Liang and Luy, 2006). This study focused on time harmonics by examining their impacts on the performance of SCIM corresponding to the skin effect.

2.1 Equivalent circuit

The following equation may be used as a general guide for calculating the harmonics produced by converter equipment on a poly-phase system:

$$h = 6k \mp 1 \qquad (1)$$

For h = 6k – 1 (h = 5, 11, 17, …) the phase sequence of the harmonic voltage is the inverse of the fundamental voltage, and is represented by the negative-sequence harmonics. For h = 6k + 1 (h = 7, 13, 19, …) Positive-sequence harmonics indicate voltages whose phase sequence is identical to that of the fundamental voltage.

The per-unit slip of an induction motor is given as

$$S = \frac{n_s - n_r}{n_s} \quad (2)$$

$$n_r = (1 - S)n_s \quad (3)$$

For any harmonic frequency, the slip can be calculated as shown below

$$S_h = \frac{\pm h n_s - (1-S)n_s}{\pm h n_s} \quad (4)$$

$$S_h = \frac{\pm h - (1-S)}{\pm h} \quad (5)$$

A positive sign refers to positive-sequence harmonics, while a negative sign refers to negative sequence harmonics.

The equivalent circuit of IMs under distorted supply is similar to that under balanced supply, with take skin effect on the parameters and with slip as a function of the fundamental. Design A, B, and D have the same equivalent circuit, which is single cage rotor slots as shown in figure 1, while design C has a different circuit because of its rotor slot shapes, which is double cage rotor slots as shown in figure 2.

Harmonics are often measured using two factors: harmonic voltage factor (HVF) and total harmonic distortion (THD). According to the IEC60034-17 standard, HVF is defined as follows:

$$HVF = \sqrt{\sum_{h=5}^{\infty} \frac{U_h^2}{h}} \quad (6)$$

Where, U_h is the ratio of the voltage of the h^{th} harmonic (V_h) to the voltage of the fundamental (V_1). h is the order of odd harmonics omitting triple h harmonics, such as h=5, 7, 11, 13, 17, 19, 23, and so on. In contrast, the IEEE-519 standard describes the total harmonic distortion of the voltage (THD_v) as follows:

$$THD_v = \sqrt{\frac{\sum_{h=2}^{\infty} V_h^2}{V_1^2}} \quad (7)$$

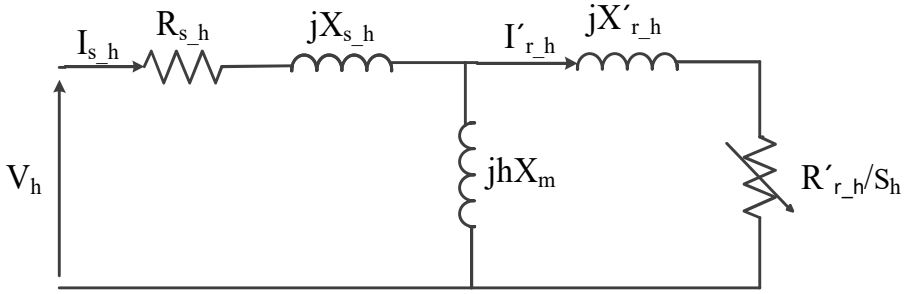

Figure 1: Per-phase Equivalent Circuit Corresponding to Harmonic Frequencies and skin effect for designs A, B&D

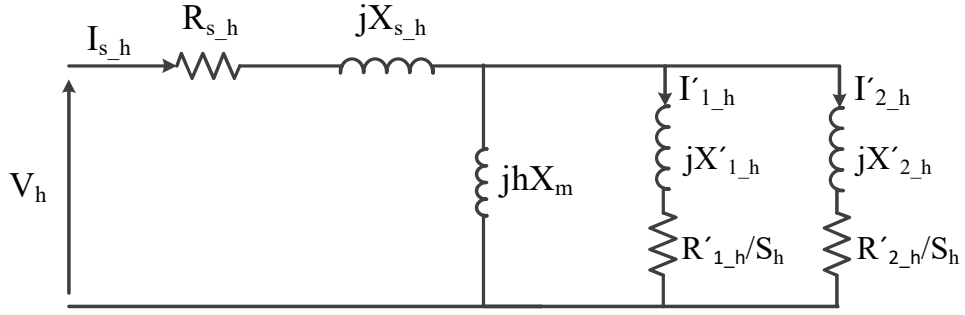

Figure 2: Per-phase Equivalent Circuit Corresponding to Harmonic Frequencies and skin effect for design C

2.2 Skin Effect

The frequency of the current flowing through the rotor bars influences the dynamic impedance of the rotor bars of IM. The skin effect is heavily influenced by the rotor bar design. It is minor in wound rotor or single cage motors and strongly evident in the deep bar and double cage motors.

When harmonics are included in the voltage supply of the motor, a larger rise in stator resistance might be predicted. According to (Buck et al., 1984), total stator winding resistance corresponding to the h^{th} harmonic may be stated as:

$$R_{s\_h} = R_{sdc}\left(1 + C_1 H_s^4 {f_h}^2\right) \quad (8)$$

With the premise that the end ring and bar DC resistances are equal, the impact of harmonics on rotor resistance may be represented as follows:

$$R_{r\_h} = R_{rdc}\left(1 + C_2 H_r \, {f_h}^{0.5}\right) \quad h>1 \quad (9)$$

Where R_{sdc} and R_{rdc} are the stator and rotor DC winding resistances, respectively, H_s and H_r are the stator and rotor slots depth in cm, respectively, f_h is the harmonic frequency ($h \times f$), the constant C_1=0.63× 10^{-8} and C_2 is a function of motor power rating and is different for various types of bar shapes depending on the cage material and temperature. C_2 has been suggested to be in the range of 0.025 to 0.05 for motors with a peak power of 10 kW or less, and 0.15 for motors with a peak power greater than 30 kW.

Because the stator leakage inductance is commonly assumed to be constant with harmonic frequency, the stator leakage reactance (X_{s_h}) is proportional to the harmonic order as follows:

$$X_{s\_h} = h \, X_s \quad (10)$$

However, due to the deep bar effect, the rotor leakage reactance decreases as the rotor current frequency increases. As a result, the rotor leakage reactance (X_{r_h}) rises with harmonic order, but not linearly, and the total effective leakage reactance can be approximated as (Jalilian, 1997):

$$X_h \approx 1.07 \, X \, h^{0.84} \quad h>1 \quad (11)$$

Where

$$X = X_s + X_r \quad (12)$$

$$X_h = X_{s\_h} + X_{r\_h} \quad (13)$$

The rotor leakage reactance can be expressed as:

$$X_{r\_h} = X_h - X_{s\_h} \quad (14)$$

2.3 Copper Losses

If the supply waveform has a high harmonic content, the extra losses caused by the presence of harmonics may be significant. These losses are caused by a rise in magnetic and ohmic losses. Harmonic main flux and harmonic leakage flux generate magnetic losses. Because the rotor slip, S_h, is close to one, harmonic current of the stator is reflected in the rotor, resulting in a low main harmonic flux. It is difficult to assess the magnetic loss in metallic components produced by harmonic leakage flux. Because of the low value of harmonic fluxes, it is thought that disregarding these losses can create insignificant inaccuracy. As a result, the magnetic loss increase is regarded as minimal, and the loss increase is mostly ascribed to the copper loss (Saleh and Radhi, 2006).

The rms value of the total current is

$$I = \sqrt{I_1^2 + \sum_{h=5,7,\ldots}^{\infty} I_h^2} \quad (15)$$

The extra copper losses in the stator are calculated by summing the losses caused by each harmonic. The total stator copper losses per phase are denoted by

$$P_s = I_s^2 \, R_s + \sum_{h=5,7,\ldots}^{\infty} I_{s\_h}^2 \, R_{s\_h} \quad (16)$$

The rotor resistance change owing to the skin effect must be considered while designing a cage-rotor induction motor, especially when using a deep-bar rotor. The rotor loss for each harmonic may be calculated. The rotor copper losses caused by each harmonic are summed together to give the total copper losses of the rotor as follows,

$$P_r = I_r^2 \, R_r + \sum_{h=5,7,\ldots}^{\infty} I_{r\_h}^2 \, R_{r\_h} \quad (17)$$

The first term is the rotor loss due to the fundamental, and the second is due to harmonics.

2.4 Developed Torque

As with the fundamental component, each harmonic component develops a torque as a result of the non-sinusoidal air-gap flux and rotor current. Depending on the harmonic order, produced torques may operate in either the forward or reverse direction. Each harmonic

produces a harmonic torque, thus it can be expressed as:

$$T_h = \frac{3I_{r\_h}^2 R_{r\_h}}{h\,\omega_s S_h} \quad (18)$$

The following equation may be used to calculate the net torque created as a result of fundamental and harmonic currents:

$$T = T_1 \pm \sum_{h=5,7,..}^{\infty} T_h \quad (19)$$

Where

$$T_1 = \frac{3I_r^2 R_r}{\omega_s S} \quad (20)$$

The positive sign denotes harmonic order torque rotates in the same direction as a fundamental torque (i.e., h=7, 13, 19, 25,...), whereas the negative sign denotes harmonic order torque rotates in the reverse direction of the fundamental torque (i.e., h=5, 11, 17, 23,...). Even though the net harmonic torques oppose the fundamental one, it is obvious that T_h is quite little and low order harmonics cause the most torque decrease.

Constant torques result from the interplay of air-gap flux and rotor current pertaining to the same harmonic. While a pulsating torque is produced as a result of the interaction of air-gap flux and rotor current of various harmonics. For instance, when a fundamental flux interacts with rotor currents of 5^{th} and 7^{th} harmonic, the pulsing torque is created at 6f1.

2.5 Derating Factor (DF)

Derating of IM refers to running the motor at a lower load than the rated load torque. If the harmonics have a large magnitude, the derating of IM might be significant. Derating is used to address difficulties with induction motor performance when the motor is fed by distorted supply. To establish the DF, the load on the motor remains constant up to the point when the stator current of IM reaches the value specified for it. DF at rated current is the ratio of output power with a distorted supply (Pout-d) to output power with a sinusoidal supply (Pout-s) (Sen and Landa, 1989):

$$DF = \frac{P_{out\_d}}{P_{out\_s}} \quad (21)$$

3. Results and Discussion

Four NEMA designs of SCIM under distorted supply conditions are analyzed and simulated by the MATLAB/SIMULINK software program. The steady-state performance of these designs under the distorted supply is investigated and compared to show which design is more affected by harmonics. This study was carried out with maintained rated voltage for difference THD_v, 15kW, 50Hz, 49.6N.m, and 2-pole three-phase Y connected for each design. The values of resistance and reactance of the stator and rotor of the A, B, C, and D designs are shown in table 1 (Pedra et al., 2006). The applied voltage to the stator are distorted by 5^{th}, 7^{th}, 11^{th}, 13^{th}, 17^{th}, 19^{th}, 23^{th}, and 25^{th} order harmonics, for six different THD_v values that are demonstrated in table 2. Figure 3 illustrates the three-phase voltage supply polluted by eight order harmonics at THD_v=25%.

Table 1: The values of parameters of each design.

Design	A	B	C	D
$R_S(\Omega)$	0.1456	0.1456	0.1456	0.1456
$R_r(\Omega)$	0.32674	0.46961	0.684(inner cage) 2.521(outer cage)	1.36
$X_S(\Omega)$	0.7681	0.7681	0.7681	0.7681
$X_r(\Omega)$	0.7681	1.1772	1.822(inner cage) 0.582(outer cage)	0.7681
$X_m(\Omega)$	33.3	33.3	33.5	33.3

Table 2: The value of THD_v with respect to harmonic order

Harmonic Order	K_h%	K_h%	K_h%	K_h%	K_h%	K_h%
5	0.0	4	8	12	16	20
7	0.0	2.5	4.5	7	9.5	12
11	0.0	1.5	2.9	4.1	5.5	7
13	0.0	0.8	2	3	4	5
17	0.0	0.5	1.25	1.7	2	2.3
19	0.0	0.3	1	1.25	1.5	1.7
23	0.0	0.2	0.5	1	1.25	1.45
25	0.0	0.15	0.3	0.5	0.7	0.9
THD_v%	0.0	5	10	15	20	25

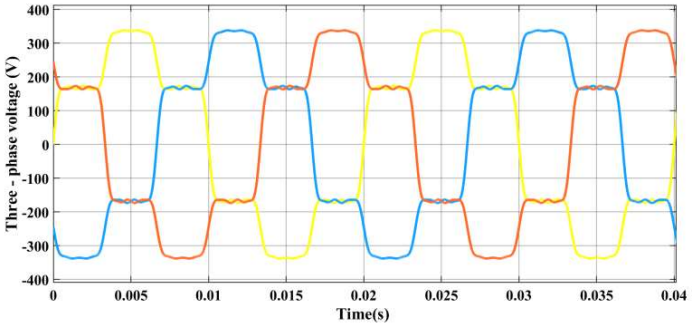

Figure 3: The three-phase non-sinusoidal supply voltage at THD_v% =25%

3.1 Torque - Speed Characteristic

To investigate the steady-state performance of the four designs of SCIMs under non-sinusoidal conditions, torque-speed characteristics have been evaluated for six different values of THD_v%, which range from 0% (sinusoidal supply) to 25% (distorted supply). Figure 4 shows the variation of developed electromagnetic torque with the rotor speed for A, B, C, and D designs at different values of THD_v%. It is clear that when the value of THD_v% is increased, the value of developed torque will decrease for each design. The amount of decreasing torque is very large in design D at standstill and in designs A, B, and C at maximum slip. Figure 5 shows how the rotor speed decreases with increasing THD_v% for each design at rated load, using both the analytical method and MATLAB simulation. The difference between the analytical and simulation results is very small, and increasing THD_v% affects the rotor speed of design D more than designs C and B, while design A is less affected by it.

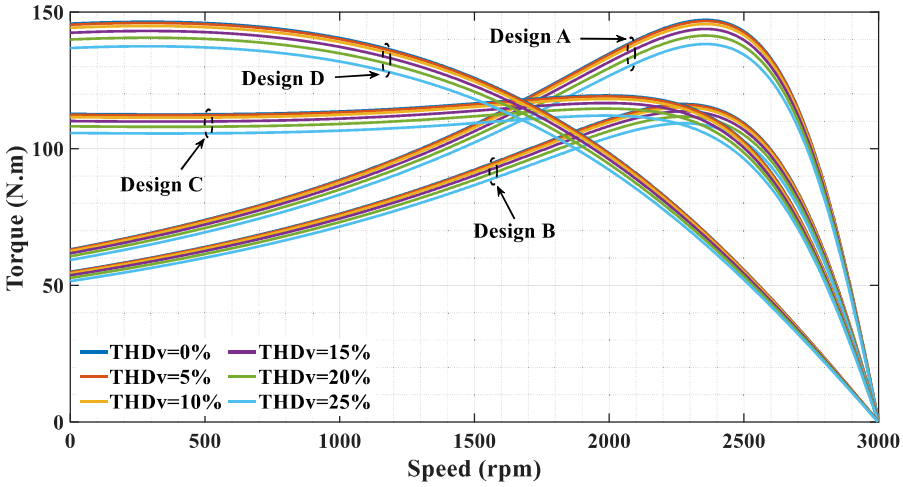

Figure 4: Torque – speed characteristic for A, B, C, and D design at different THD_v.

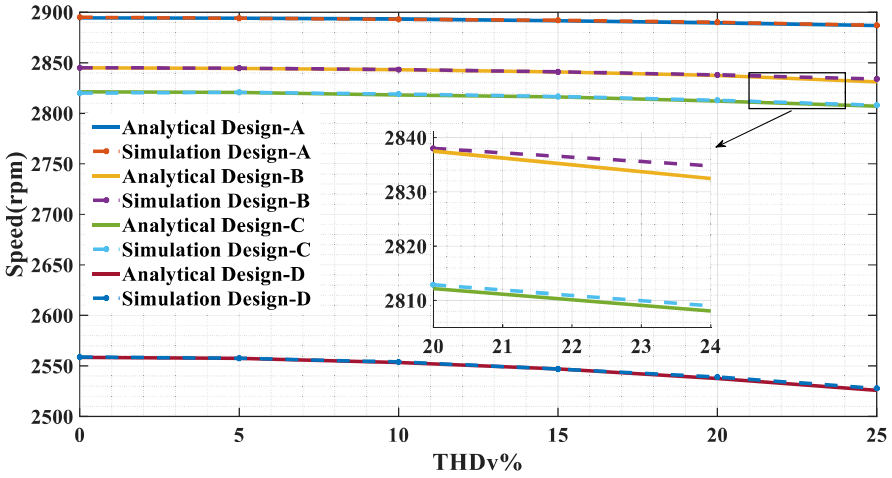

Figure 5: Rotor speed versus THD_v for each design at rated load.

3.2 Stator and Rotor current

When IM is fed from a distorted supply, the stator and rotor current will increase. Figures 6 and 7 show the variation of stator and rotor current with THD_v% at rated load for each design, respectively. To measure the effective value of the harmonic components of a current waveform, THD-I is used. Figures 8 and 9 represent THD-I_s% and THD-I_r% versus THD_v% at rated load for each design.

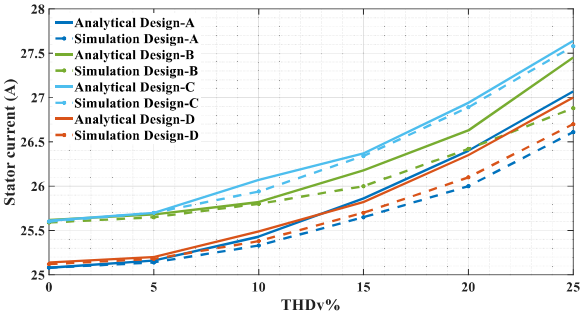

Figure 6: Stator current versus THD_v for each design .

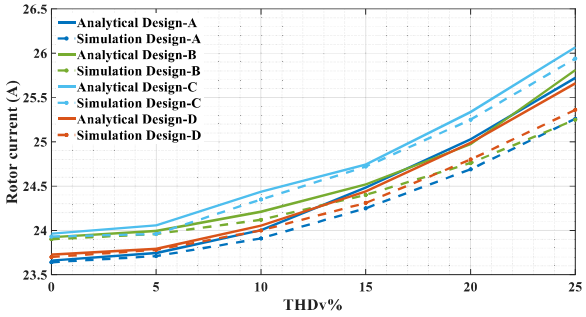

Figure 7: Rotor current versus THD_v for each design.

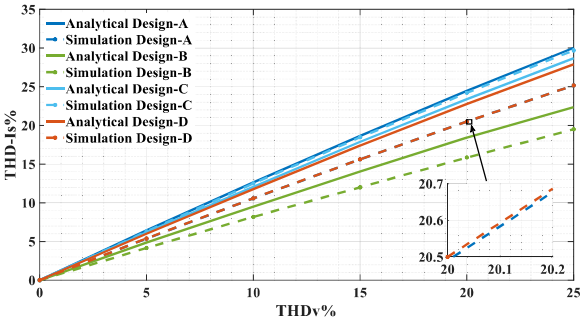

Figure 8: THD-I_s versus THD_v for each design.

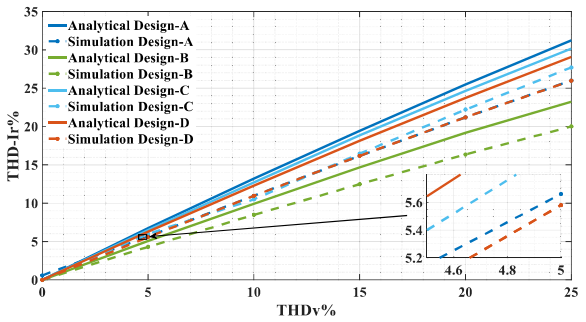

Figure 9: THD-I_r versus THD_v for each design.

3.3 Copper Losses

There are several losses in IM, such as stator and rotor copper losses, iron losses, mechanical losses, and so on. In this study, copper losses have been analyzed with the assumption of constant others. The percentage increase of stator and rotor copper losses versus THD_v% at full load for each design is shown in figures 10 and 11, respectively. Figure 12 shows the percentage increase of total copper losses versus THD_v% for the four designs at full load. It is clear that design C is more affected by harmonics.

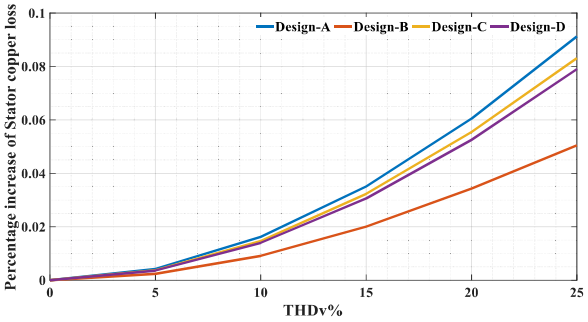

Figure 10: Percentage increase of stator copper loss versus THD_v for each design.

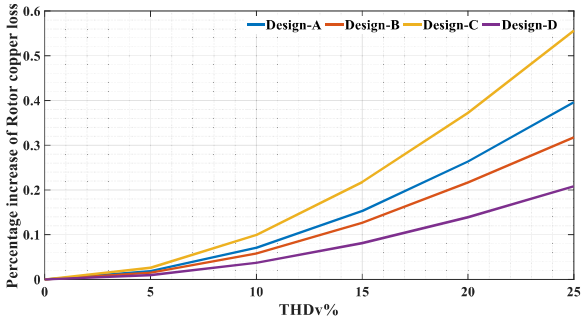

Figure 11: Percentage increase of rotor copper loss versus THD_v for each design.

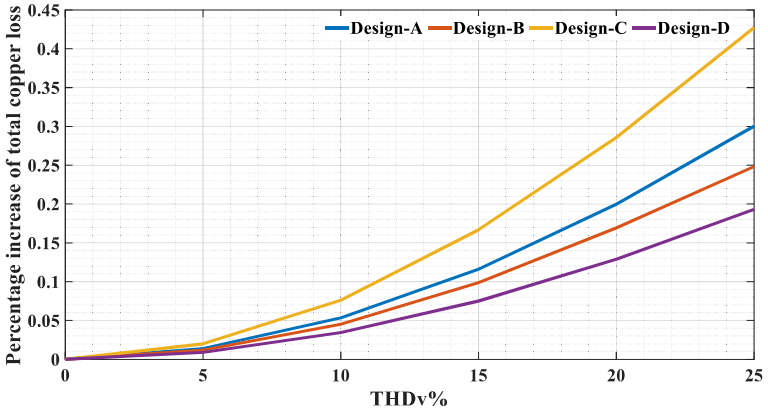

Figure 12: Percentage increase of total copper loss versus THD_v for each design.

3.4 Efficiency, Power Factor, and Derating Factor

NEMA designs are different in efficiency because their rotor constructions are different; design A has a higher efficiency than designs B, C, and D, respectively. The distorted supply affected the efficiency of each design. Figure 13 shows the relationship between efficiency and THD_v% of each design at rated load. Increasing THD_v% will cause a decrease in efficiency. This decrease is more in design C as compared to other designs because design C has a double cage rotor slot, and it is more affected by harmonic frequency. The variation of efficiency and power factor with different motor loads (25%, 50%, 75%, and 100% of full load) at six values of THD_v% for each design are shown in figures 14 and 16, respectively. In figure 15, power factor versus THD_v% at full load is illustrated; increasing THD_v% will cause a decrease in power factor, especially in design A.

The decreasing derating factor with increasing HVF% is shown in figure 17. It is clear that design C is more affected by harmonics as compared to other designs, which decrease from 1 to 0.87 when HVF% increases from 0 to 10.35%.

Table (3) shows the variation of settling time (T_s), rising time (T_r), torque pulsation, and speed ripple at different THD_v% for designs A, B, C, and D at half and full load operation. It can be seen that with increasing THD_v%, the T_s, T_r, torque pulsation, and the ripple of rotor speed are

increased for all designs. Also, it can be noted that designs C and D have less T_s and T_r, while design B has minimum torque pulsation and speed ripples. The time required to reach the steady state operation in designs C and D refers to high introduce dynamic resistance in the rotor circuit.

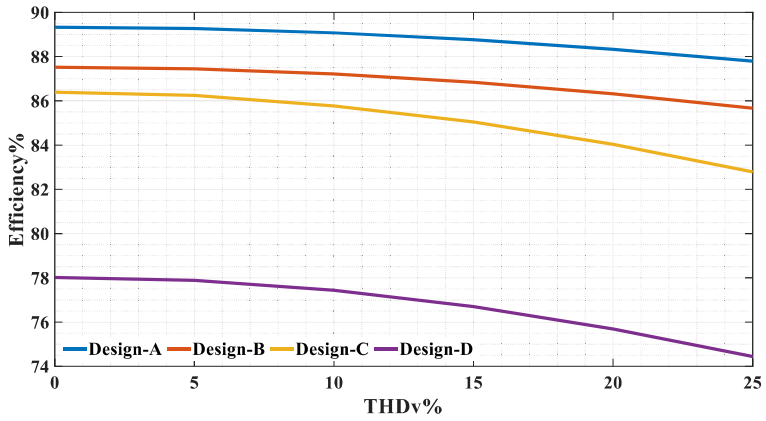

Figure 13: Efficiency versus THD_v for each design at full load.

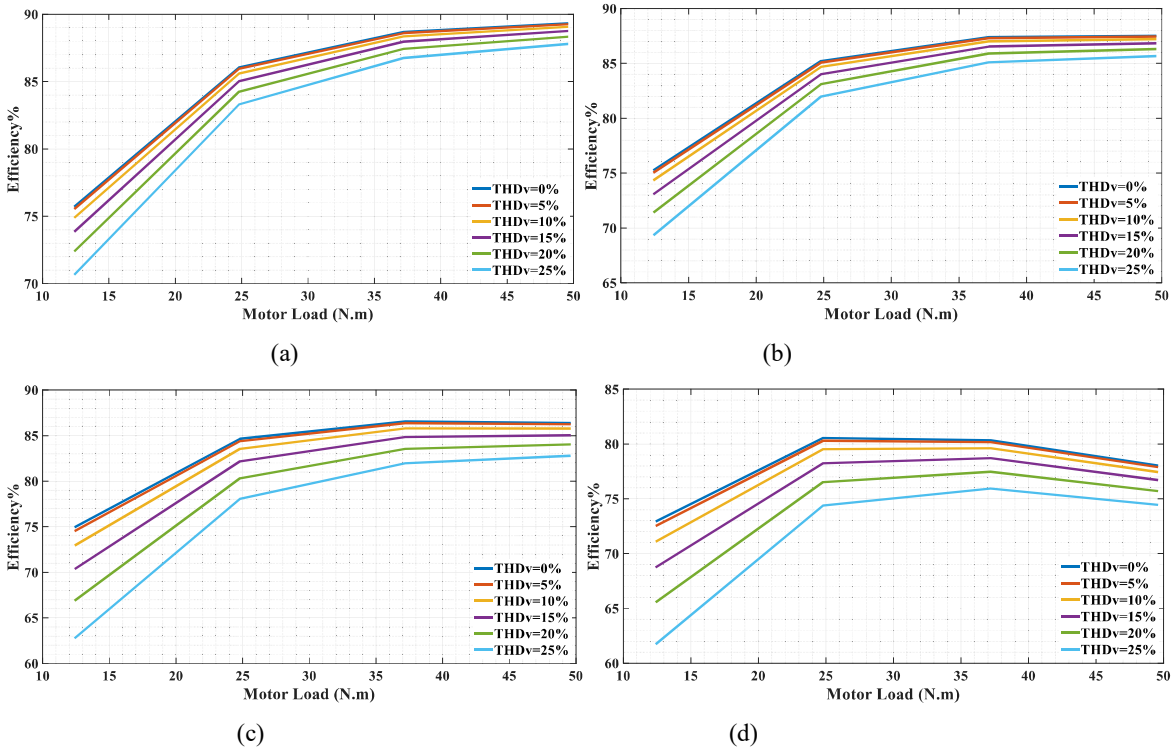

Figure 14: Efficiency versus motor load at different THD_v (a) Design A. (b) Design B. (c) Design C. (d) Design D.

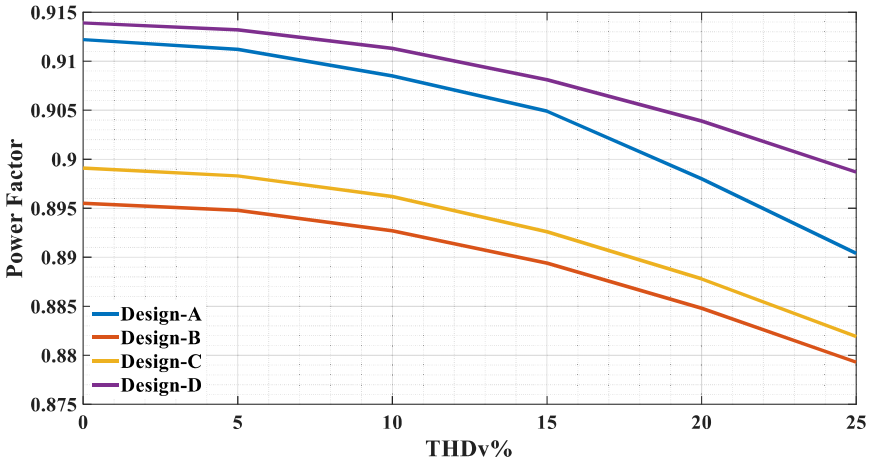

Figure 15: Power factor versus THD_v for each design at rated load.

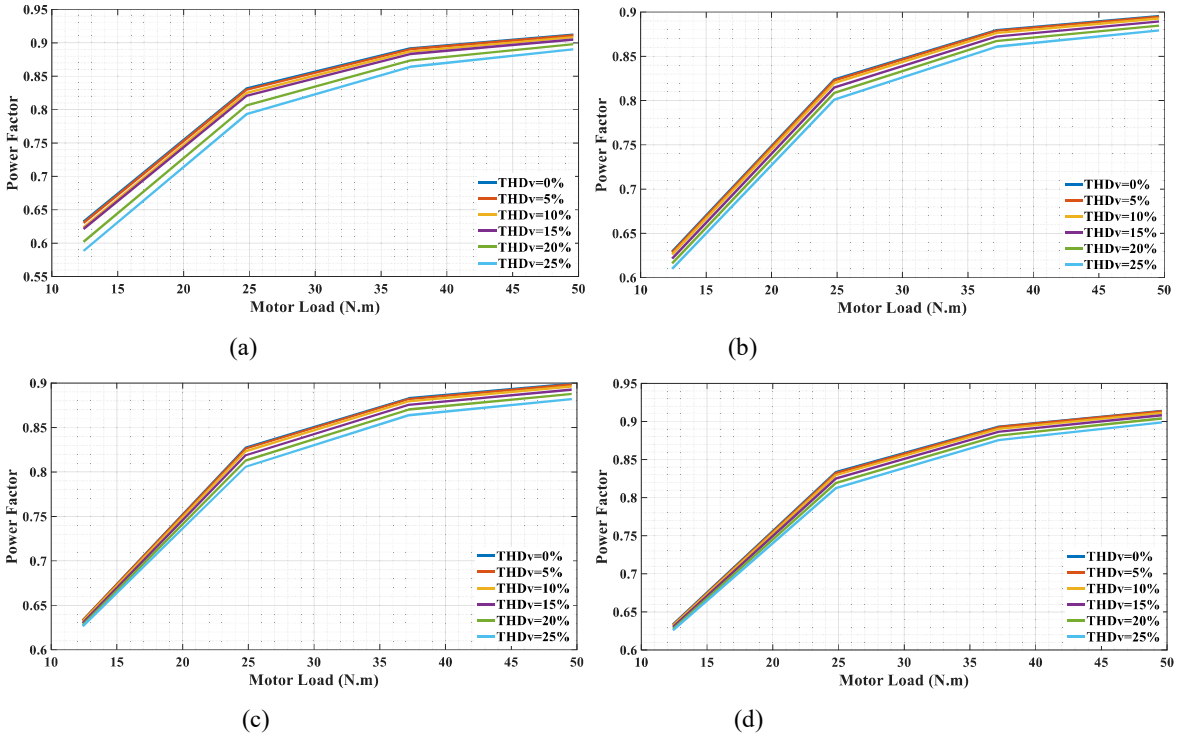

Figure 16: Power factor versus motor load at different THD_v (a) Design A. (b) Design B. (c) Design C. (d) Design D.

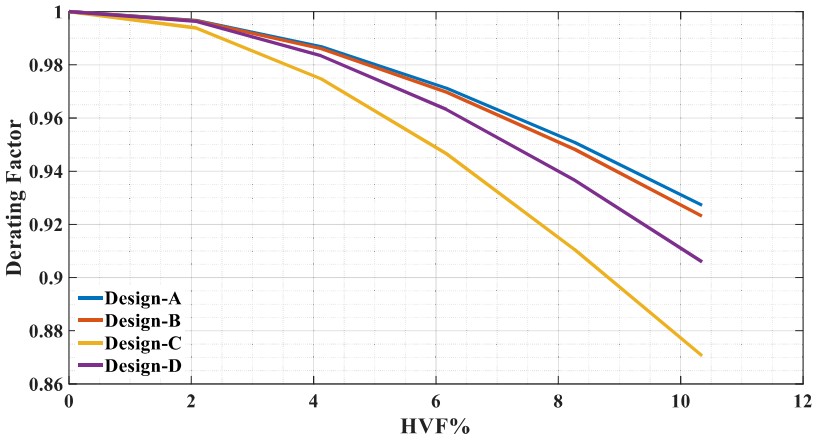

Figure 17: Derating factor versus HVF% for each design.

Table 3: The variation of T_s, T_r, torque pulsation, and speed ripple versus THD_v% at half and full load for different NEMA designs.

Design	THD_v%	half load				full load			
		T_s(ms)	T_r(ms)	Torque pulsation (N.m)	Speed ripple (rpm)	T_s(ms)	T_r(ms)	Torque pulsation (N.m)	Speed ripple (rpm)
A	0	540	282	0	0	850	344	0	0
	5	550	286	2.9	0.3	865	350	3	0.3
	10	560	292	6.1	0062	890	353	6.1	0.63
	15	570	293	8.5	0.88	930	356	8.7	0.9
	20	580	296	11.18	1.15	960	361	11.6	1.17
	25	590	300	13.75	1.4	995	383	14.13	1.44
B	0	575	311	0	0	1223	467	0	0
	5	585	313	2.3	0.23	1248	470	2.3	0.25
	10	595	315	4.8	0.49	1295	474	4.9	0.5
	15	605	319	6.8	0.69	1372	481	7.1	0.72
	20	620	323	8.75	0.9	1495	516	9.2	0.9
	25	650	327	10.8	1.1	1690	546	11.3	1.15
C	0	380	186.9	0	0	418	251.6	0.28	0.08
	5	385	189	3.4	0.34	425	254.6	3.6	0.4
	10	390	192.3	7.2	0.47	430	261	7	0.78
	15	400	196.5	10.1	1	435	267.6	9.4	1
	20	405	202	13	1.35	438	278	12.6	1.3
	25	410	208.1	16.1	1.6	443	292.2	15.6	1.5
D	0	585	203	0	0	665	243	0	0
	5	600	209	2.84	0.28	670	252	2.8	0.29
	10	606	214	6	0.61	675	256	5.9	0.6
	15	610	217	8.2	0.86	687	260	8.3	0.85
	20	625	220	10.89	1.12	695	264	10.8	1.12
	25	630	224	13.37	1.36	710	278	13.35	1.37

4. Conclusion

The influence of voltage distortion upon the steady-state performance of each of the NEMA designs: A, B, C, and D induction motors have been studied in this paper using an analytical method. The analytic study presented in this paper allows the effect of supply harmonic distortion from THD_v of (0–25) %. The results of the study show that the electromagnetic developed torque, the rotor speed, the power factor, the efficiency, the stator and rotor currents depend on the level of supply distortion for each NEMA design and have a negative impact on each of them. Also, it can be investigated that the design C induction motor is more sensitive than the other designs because it has been affected by the skin effect, and the response time for design C to reach steady-state operation is less. The MATLAB/Simulink software has been used to validate the steady-state performance of different NEMA designs under non-sinusoidal supply conditions.

Reference

AMEEN, H. & AULA, F. 2021. Performance Analysis of the Slip Power Recovery Induction Motor Drive System Under Unbalance Supply Voltages. *Advances in Electrical and Electronic Engineering,* 19.

BELEIU, H., MAIER, V., PAVEL, S., BIROU, I., PICA, C. & COSMIN, D. 2020. Harmonics Consequences on Drive Systems with Induction Motor. *Applied Sciences,* 10**,** 1528.

BUCK, F., GIUSTELINCK, P. & BACKER, D. 1984. A Simple But Reliable Loss Model for Inverter-Supplied Induction Motors. *Industry Applications, IEEE Transactions on,* IA-20**,** 190-202.

DEBRUYNE, C., DERAMMELAERE, S., DESMET, J. & VANDEVELDE, L. Comparative study of the influence of harmonic voltage distortion on the efficiency of induction machines versus line start permanent magnet machines. 2012 IEEE 15th International Conference on Harmonics and Quality of Power, 17-20 June 2012 2012. 342-349.

DELEANU, S., IORDACHE, M., STANCULESCU, M. & NICULAE, D. The Induction Machine Operating from a Voltage Supply, Unbalanced and Polluted with Harmonics: A Practical Approach. 2019 15th International Conference on Engineering of Modern Electric Systems (EMES), 13-14 June 2019 2019. 181-184.

DERAZ, S. A. & AZAZI, H. Z. Impact of distorted voltage on three-phase induction motor performance. 2017 Nineteenth International Middle East Power Systems Conference (MEPCON), 19-21 Dec. 2017 2017. 857-863.

DONOLO, P., BOSSIO, G., DE ANGELO, C., GARCÍA, G. & DONOLO, M. 2016. Voltage unbalance and harmonic distortion effects on induction motor power, torque and vibrations. *Electric Power Systems Research,* 140.

DONOLO, P. D., PEZZANI, C. M., BOSSIO, G. R., DE ANGELO, C. H. & DONOLO, M. A. J. I. T. O. I. A. 2020. Derating of induction motors due to power quality issues considering the motor efficiency class. 56**,** 961-969.

GNACIŃSKI, P. & KLIMCZAK, P. 2020. High-Power Induction Motors Supplied with Voltage Containing Subharmonics. *Energies,* 13**,** 5894.

HILMI, A. & FADHIL, A. 2021. Performance Analysis and Modeling of SRRCCIM under the Impact of Unbalance Supply Voltage. *Journal of Electrical and Electronics Engineering,* 14**,** 5-10.

JALILIAN, A. 1997. Calorimetric measurement of induction motor harmonic losses.

JASSIM, A., HUSSEIN, A. & ABBAS, L. 2021. Study the performance of three-phase induction motor under imbalanced non-sinusoidal supply. *IOP Conference Series: Materials Science and Engineering,* 1058**,** 012035.

LERCH, T. & RAD, M. 2016. Influence of higher harmonics on losses in induction machines. *TECHNICAL TRANSACTIONS 1897-6301,* 13**,** 13-24.

LIANG, X. & LUY, Y. Harmonic Analysis for Induction Motors. 2006 Canadian Conference on Electrical and Computer Engineering, 7-10 May 2006 2006. 172-177.

LORDOGLU, A., GULBAHCE, M. & KOCABAS, D. 2021. A Comprehensive Disturbing Effect Analysis of Multi-Sectional Rotor Slot Geometry for Induction Machines in Electrical Vehicles. *IEEE Access,* PP**,** 1-1.

NEAPOLITAN, R. E. & NAM, K. H. 2018. *AC motor control and electrical vehicle applications*, CRC press.

NEVES, A. B. F., MENDONÇA, M. V. B. D., FILHO, A. D. L. F. & ROSA, G. Z. Effects of voltage unbalance and harmonic distortion on the torque and efficiency of a Three-Phase Induction Motor. 2016 17th International Conference on Harmonics and Quality of Power (ICHQP), 16-19 Oct. 2016 2016. 943-948.

PEDRA, J., SAINZ, L. & CÓRCOLES, F. 2006. Harmonic modeling of induction motors. *Electric Power Systems Research,* 76**,** 936-944.

RUTHES, J. R., NAU, S. L. & NIED, A. Performance analysis of induction motor under non-sinusoidal supply voltages. 2016 12th IEEE International Conference on Industry Applications (INDUSCON), 20-23 Nov. 2016 2016. 1-6.

SALEH, A. & RADHI, A. 2006. EFFECT OF HARMONICS ON A SOLID-ROTOR INDUCTION MOTOR. *University of Baghdad Engineering Journal,* 12**,** 199-217.

SEN, P. K. & LANDA, H. A. Derating of induction motors due to waveform distortion. Industrial Applications Society, 36th Annual Petroleum and Chemical Industry Conference, 1989. IEEE, 29-34.

TEZCAN, M., YETGIN, A., CANAKOGLU, A., CEVHER, B., TURAN, M. & AYAZ, M. 2018. Investigation of the effects of the equivalent circuit parameters on induction motor torque using three different equivalent circuit models. *MATEC Web of Conferences,* 157**,** 01019.

ZHANG, D., AN, R. & WU, T. 2017. Effect of Voltage Unbalance and Distortion on the Loss Characteristics of Three Phase Cage Induction Motor. *IET Electric Power Applications,* 12.